Nonlinear theory and experiment of collective free electron lasers

Jonathan S. Wurtele and Ronson Chu
Department of Physics and Plasma Fusion Center, Massachusetts Institute of Technology, Cambridge, Massachusetts 02139

Joel Fajans
Department of Physics, University of California–Berkeley, Berkeley, California 94720

(Received 13 November 1989; accepted 19 March 1990)

A theoretical and experimental study of the nonlinear performance of a free electron laser (FEL) amplifier operating in the collective (Raman) regime is reported. The FEL generates up to ~ 100 kW of rf power at a frequency of 9.3 GHz and an efficiency of $\sim 10\%$. Power saturation, efficiency, and synchrotron oscillations are studied as a function of rf input power, electron beam energy, current, wiggler field amplitude, and axial distance within the helical wiggler. The influences of the nonlinear electron motion in the ponderomotive potential and space-charge waves are studied by measurements of the dependence of gain and efficiency on the initial radiation intensity. Good agreement with a nonlinear theory that takes cognizance of electron trapping in the combined ponderomotive and space-charge potential well is obtained.

I. INTRODUCTION

Free electron lasers (FEL's) are currently under investigation because of their remarkable properties, which include their high efficiencies and output powers, their potential as coherent short wavelength sources, and their inherent frequency tunability. Subsequent to the original envisioning[1,2] of the FEL and the first proof-of-principle experiments,[3] detailed comparisons of experiment and theory have been made in the linear[4,5] and nonlinear regimes.[6,7]

In this paper we study the nonlinear behavior of a microwave FEL. The small signal linear gain behavior of this device, previously investigated,[5] is now well understood. Further investigations found good agreement between numerical simulation and measurements of the nonlinear amplitude and phase of the rf wave.[6] Here we examine the influence of rf input power on the saturation and detuning characteristics of the laser, and examine that power as a function of the beam current and the wiggler field amplitude and length. The physics of our collective FEL is well described by electron trapping in the potential formed by the combined action of the ponderomotive and self-consistent space-charge forces.

The major differences between the microwave regime FEL theory studied here and the standard optical (Compton) regime FEL theory[8–10] are corrections for the excitation of a collective space-charge wave on a finite radius beam propagating in a waveguide, the transverse structure of the waveguide mode,[11,12] three-dimensional wiggler fields, the presence of an axial guide magnetic field, and the relatively low velocity ($v/c \sim 0.6$) of the electron beam. Three-dimensional effects are included by using appropriately calculated coupling coefficients as input parameters and solving transcendental expressions for the transverse electron motion.[13] These extended one-dimensional model input parameters are found analytically through the evaluation of the overlap between the waveguide mode and electron beam, and the evaluation of space-charge reduction factors.

The FEL equations are solved using a numerical simulation that tracks macroparticles in a single ponderomotive wavelength. The simulation is itself one dimensional, and propagates only the TE_{11} waveguide mode. There are no adjustable parameters. Some portions of this paper expand on comparisons between experiment and theory reported earlier,[6,8] and others report new studies of the influence of input wave power on the FEL efficiency and gain.

In Sec. II we derive our nonlinear model and numerical simulation. Section III contains the linearization of the model and comparison with previous linear theories. In Sec. IV we discuss the space-charge wave, which is particularly important in our parameter regime. In Sec. V the experimental and theoretical results are compared, and the first measurements of the shift in optimum detuning and changes in efficiency scaling that result from increasing the rf input power are reported.

II. DERIVATION OF THE NONLINEAR MODEL

In this section we derive the nonlinear model of the FEL for the parameter regime of our microwave FEL experiment. The model couples single particle orbits in combined helical and axial magnetic fields with the slowly varying amplitude and phase of the TE_{11} mode in a circular waveguide. The nonlinear equations of motion are one dimensional, but allow for the effects of transverse field variations through the evaluation of waveguide mode-beam overlap integrals and space-charge reduction factors. The influence of the three-dimensional wiggler fields on the electron orbits is analyzed by solving the well-known transcendental equations relating the energy γ and the normalized perpendicular and parallel velocities $\beta_\perp$ and $\beta_\parallel$ for an electron on an ideal orbit. We do not assume that $\gamma \gg 1$.

A. Particle equations

Electrons orbit in the combined axial magnetic field,

$$\mathbf{B}_0 = B_0 \hat{\mathbf{z}}, \tag{1}$$

and the helically polarized wiggler field given by

 0899-8221/90/071626-09$02.00

$$\mathbf{B}_w(r,\phi,z) = 2B_w\{-I_1'(\lambda)\sin(k_w z-\phi)\hat{\mathbf{r}} + [I_1(\lambda)/\lambda] \times\cos(k_w z-\phi)\hat{\phi} - I_1(\lambda)\cos(k_w z-\phi)\hat{\mathbf{z}}\}, \tag{2}$$

where $\lambda = k_w r$, $k_w = 2\pi/l$ is the wiggler wave number, I_1 is the modified Bessel function, the prime denotes derivative with respect to the total argument, and we use cylindrical coordinates (r,ϕ,z). Neglecting the influence of the radiation field, and assuming an ideal wiggler entrance, the electron orbits are described by[5]

$$\boldsymbol{\beta}_\perp = \beta_\perp[\sin(k_w z-\phi)\hat{\mathbf{r}} - \cos(k_w z-\phi)\hat{\phi}], \tag{3}$$

where the normalized perpendicular velocity $\beta_\perp$ is found from the simultaneous solution of the equations

$$\frac{\beta_\perp}{\beta_\parallel} = \frac{2\Omega_w c k_w I_1(\lambda)/\lambda}{c\beta_\parallel k_w\gamma - \Omega_0 - 2\Omega_w c k_w I_1(\lambda)} \tag{4}$$

and

$$\beta_\parallel = \sqrt{1-1/\gamma^2-\beta_\perp^2}. \tag{5}$$

In Eq. (4), the velocities $\beta_\perp$ and $\beta_\parallel$ are normalized by the speed of light c, Ω_w, Ω_0 are the wiggler and axial cyclotron frequencies, $\gamma = 1 + eV/m_0c^2$ is the beam energy, and $\lambda = \beta_\perp/\beta_\parallel = \pm k_w r$ is the normalized size of the orbit, with $\lambda = -k_w r$ if $\Omega_0 > \gamma k_w \beta_\parallel c$ and $\lambda = +k_w r$, if $\Omega_0 < \gamma k_w \beta_\parallel c$. We assume that electrons remain on these orbits during the FEL interaction, neglecting the detailed effects of the precession due to off-axis injection[14] and emittance; this is a good approximation for the high quality electron beam used in this experiment. In addition, the direct influence of the radiation field on the perpendicular motion is very small for the low powers at which this FEL operates. Thus the radiation field influences the particle motion only through the energy relation $d\gamma/dt \sim \mathbf{v}\cdot\mathbf{E}$; consequently, the perpendicular and parallel energies evolve so that the electron stays on the orbit given by Eqs. (4) and (5).

With the time t replaced by the axial position z as the independent variable, the electron (charge $-e$, mass m_0) energy evolves according to

$$\frac{d\gamma}{dz} = -\frac{e}{m_0c^2}\frac{\beta_\perp}{\beta_\parallel}\frac{A(z)Z_0k_0}{k_\perp}\left(\frac{J_1(\alpha)}{\alpha}\sin[k_w z-\phi(z)] \times\cos[\theta_s+\phi(z)] + J_1'(\alpha)\cos[k_w z-\phi(z)] \times\sin[\theta_s+\phi(z)] - \frac{e}{m_0c^2}E_z\right), \tag{6}$$

where $\theta_s = k_z z + \varphi(z) - \omega t(z)$, the amplified wave frequency, axial wave number, and perpendicular wave number are given by ω, k_z, and $k_\perp$, respectively, $k_0 = \omega/c$ is the normalized frequency, E_z is the axial component of the electric field due to the beam bunching, $\alpha = k_\perp r$, the impedance of free space is Z_0, and J_1 is a Bessel function. In deriving Eq. (6), the transverse components of the waveguide mode are taken from Table I. Furthermore, the amplified wave amplitude $A(z)$ and phase $\varphi(z)$ are assumed to be slowly varying on the spatial scale $\lambda_s = 2\pi c/\omega$. The radial space-charge field also contributes to the electron motion, but does not generate a large slowly varying term in the energy equation. As described below, the expression for E_z includes the influence of the conducting waveguide wall through an appropriately calculated coupling parameter.

TABLE I. TE_{11} waveguide mode.

TE_{11} waveguide mode field components	
E_r	$A(z)(k_0Z_0/k_1^2 r)J_1(k_\perp r)\cos(\theta_s+\phi)$
E_ϕ	$-A(z)(k_0Z_0/k_\perp)J_1'(k_\perp r)\sin(\theta_s+\phi)$
E_z	0
H_r	$A(z)(k_z/k_\perp)J_1'(k_\perp r)\sin(\theta_s+\phi)$
H_ϕ	$A(z)(k_z/k_1^2 r)J_1(k_\perp r)\cos(\theta_s+\phi)$
H_z	$-A(z)J_1(k_\perp r)\cos(\theta_s+\phi)$
	$Z_{11} = k_0Z_0/k_z$
	$p_{11}' = 1.841 = k_\perp r_g$
Power	$A^2(z)Z_{11}k_z^2\pi(p_{11}'^2-1)J_1^2(p_{11}')/2k_\perp^4$

For our experiment, the electron beam is small compared to the radial gradients in the transverse radiation field, so that $\alpha \ll 1$ (typically, $\alpha \approx 0.36$). With the simplification that $J_1(\alpha) \approx \alpha/2$, the energy equation reduces to

$$\frac{d\gamma}{dz} = -\frac{e}{m_0c^2}\frac{\beta_\perp}{\beta_\parallel}\frac{A(z)Z_0k_0}{2k_\perp}\sin\psi - \frac{e}{m_0c^2}E_z, \tag{7}$$

where ψ is the slowly varying phase of the particle in the ponderomotive wave. It is convenient to introduce the dimensionless field amplitude

$$a_s = \sqrt{PZ_0}/(m_0c^2/e) \tag{8}$$

and the length scale

$$C = \left(\frac{k_0p_{11}'^2}{2\pi k_z r_g^2(p_{11}'^2-1)J_1^2(p_{11}')}\right)^{1/2}, \tag{9}$$

where r_g is the waveguide radius, p_{11}' is the first zero of $J_1'(z)$, and P is the EM wave power. With these definitions, the electron energy and phase evolve according to

$$\frac{d\gamma}{dz} = -C\frac{\beta_\perp}{\beta_\parallel}a_s\sin\psi - \frac{e}{m_0c^2}E_z \tag{10}$$

and

$$\frac{d\psi}{dz} = k_w + k_z - \frac{\omega}{c\beta_\parallel} + \frac{d\varphi}{dz}. \tag{11}$$

B. Field equations

The Maxwell equation

$$-\nabla^2\mathbf{E} + \nabla(\nabla\cdot\mathbf{E}) - \frac{\omega^2}{c^2}\mathbf{E} = -\mu_0\frac{\partial\mathbf{J}}{\partial t} \tag{12}$$

for the electric field can be simplified by assuming that the electric field is composed of a vacuum waveguide mode with a slowly varying amplitude and phase, as shown in Table I, and a space-charge field, $\mathbf{E}_{sc}(\phi,r,z)$, which has a slow z dependence as well. The divergence free electric field of the TE_{11} mode satisfies

$$-\nabla^2\mathbf{E}-\frac{\omega^2}{c^2}\mathbf{E}=2k_z\frac{Z_0k_0}{k_\perp}\left(-\frac{J_1(k_\perp r)}{k_\perp r}\sin(\theta_s-\phi)\hat{\mathbf{r}}+J_1'(k_\perp r)\cos(\theta_s-\phi)\hat{\phi}\right)\frac{dA}{dz}-2k_zA\frac{Z_0k_0}{k_\perp}$$
$$\times\left(\frac{J_1(k_\perp r)}{k_\perp r}\cos(\theta_s-\phi)\hat{\mathbf{r}}+J_1'(k_\perp r)\sin(\theta_s-\phi)\hat{\phi}\right)\frac{d\varphi}{dz}=-\mu_0\frac{\partial\mathbf{J}}{\partial t}. \tag{13}$$

Note that the vacuum relation $\omega^2/c^2=k_0^2=k_z^2+k_\perp^2$ has been used.

The current can be expressed as a function of z,

$$\mathbf{J}=-e\sum_i\boldsymbol{\beta}_i(z)\delta[\mathbf{r}_\perp-\mathbf{r}_{wi}(z)]\delta[t-t_i(z)][\beta_{\parallel i}(z)]^{-1}, \tag{14}$$

where $\mathbf{r}_{wi}(z)$ is the transverse position of a particle, the index i is a particle label, and $\beta_\perp$ and $\beta_\parallel$ are found from Eqs. (4) and (5). Multiplication of Eq. (13) by

$$\{-[J_1(k_\perp r)/k_\perp r]\sin(\theta_s-\phi)\hat{\mathbf{r}}+J_1'(k_\perp r)\cos(\theta_s-\phi)\hat{\phi}\},$$

using Eq. (14), and integrating over the waveguide cross section, yields

$$\frac{k_0k_zZ_0}{k_\perp^3}\pi(p_{11}'^2-1)J_1^2(p_{11}')\frac{dA}{dz}=\frac{\omega\mu_0I}{2}\left\langle\frac{\beta_{\perp i}}{\beta_{\parallel i}}\sin\psi_i\right\rangle, \tag{15}$$

where I is the current. The average of a function F of the particle variables $(\beta_\perp,\beta_\parallel,\gamma,\psi)$ is defined as

$$\langle F(\beta_\perp,\beta_\parallel,\gamma,\psi)\rangle=\frac{1}{N_p}\sum_{i=1}^{N_p}F(\beta_{\perp i},\beta_{\parallel i},\gamma_i,\psi_i), \tag{16}$$

where N_p is the number of particles in one ponderomotive wavelength.

In terms of the normalized variables,

$$\frac{da_s}{dz}=\frac{2\pi CI}{I_A}\left\langle\frac{\beta_\perp}{\beta_\parallel}\sin\psi\right\rangle, \tag{17}$$

where C is defined in Eq. (9), and $I_A=17$ kA is the Alfvén current. The phase evolution is found through multiplication of Eq. (13) by the factor

$$\{[J_1(k_\perp r)/k_\perp r]\cos(\theta_s-\phi)\hat{\mathbf{r}}+J_1'(k_\perp r)\sin(\theta_s-\phi)\hat{\phi}\},$$

and integration over the waveguide cross section, to be

$$\frac{d\varphi}{dz}=\frac{2\pi CI}{I_Aa_s}\left\langle\frac{\beta_\perp}{\beta_\parallel}\cos\psi\right\rangle. \tag{18}$$

The space-charge wave field, which results from the beam bunching at the ponderomotive wavelength, is assumed to be of the form

$$\mathbf{E}_{sc}=\sum_n\mathbf{E}_{nc}(\mathbf{x}_\perp,z)\cos n\psi+\mathbf{E}_{ns}(\mathbf{x}_\perp,z)\sin n\psi, \tag{19}$$

where the axial variation of E_{ns} and E_{nc} is slow compared to the radiation wavelength. The z component of the space-charge wave then evolves from Eq. (12) as

$$\left(\nabla^2+\frac{\omega^2}{c^2}\right)E_z=\frac{1}{\epsilon_0}\left(\frac{\partial\rho}{\partial z}+\mu_0\epsilon_0\frac{\partial J_z}{\partial t}\right). \tag{20}$$

By expanding the current and density in a series such as that in Eq. (19), using the continuity equation, and equating the Fourier components on both sides of Eq. (20), it can be shown that

$$\left(1-\frac{\gamma_p^2}{n^2(k_z+k_w)^2}\nabla_\perp^2\right)E_{znc}=-\frac{\rho_{ns}}{\epsilon_0n(k_z+k_w)}, \tag{21}$$

$$\left(1-\frac{\gamma_p^2}{n^2(k_z+k_w)^2}\nabla_\perp^2\right)E_{zns}=\frac{\rho_{nc}}{\epsilon_0n(k_z+k_w)}, \tag{22}$$

where n is the harmonic number, ρ_{nc} and ρ_{ns} are the Fourier components of the charge density ρ, $\gamma_p=1/\sqrt{1-v_p^2/c^2}$, and $v_p=\omega/(k_z+k_w)$ is the phase velocity of the ponderomotive wave.

For the sake of simplicity, the normalized electric field that enters the simulation is not found by solving the above equations for E_z. Instead, as in earlier works,[4,6] a space-charge reduction factor p_1 is utilized. This factor, which is ~0.5 for the parameters of our experiment, can be found in the literature[15] (with corrections for $\gamma>1$) for the case of an unbunched electron beam with a uniform density profile. Recently, several careful treatments of the space-charge wave in the FEL have been made.[16–18] All of these treatments indicate that the model presented here is quite satisfactory for the parameter regime of this experiment. The electric field used in the one-dimensional simulation presented here is then

$$\frac{E_z}{m_0c^2/e}=\frac{2p_1^2\omega_{p0}^2}{c^2(k_z+k_w)}\times\sum_{n=1}^{N_h}\frac{\langle\sin n\psi\rangle\cos n\psi-\langle\cos n\psi\rangle\sin n\psi}{n}, \tag{23}$$

where n is the harmonic number, r_e is the radius of the beam, $\omega_{p0}^2=e^2n_0/\epsilon_0m_0$, and $n_0=I/ec\pi r_e^2\beta_{\parallel0}$. For the parameters of interest here, the factor p_1 varies only slightly for differing harmonics n. In general, p_1 cannot be removed from the summation and will be a function of n. For experiments with strong space-charge forces, such as the one herein, the use of only the first harmonic will lead to erroneous results in the nonlinear regime.

In summary, Eqs. (4), (5), (10), (11), (17), (18), and (23) constitute the model of the FEL that is implemented numerically in this study of nonlinear FEL phenomena. The simulation assumes that as the electrons exchange energy with the wave, they do not deviate from the ideal wiggler orbits given by the solution to Eqs. (4) and (5). We ignore the influence of the transverse gradients of both the radiation field and the space-charge wave on the amplitude of the perpendicular motion. Note that since $\lambda=k_wr_e<1$, $I_1(\lambda)\approx\lambda/2$, the right-hand side of Eq. (4) is only a weak function of λ unless the electron is close to resonance. As the power approaches saturation, the fundamental ($n=1$) and

the harmonics ($n>1$) of the space-charge wave generate rather complicated particle orbits.

III. LINEARIZED EQUATIONS

The FEL interaction can be described by particle bunching in the ponderomotive wave coupled to concomitant field growth driven by the synchronous component of the current density. The bunching arises primarily from the phase change due to an energy shift. Linearization of the single particle model with space charge has been performed for planar and helical wigglers[19] and for the circular wiggler,[20] but not for the helical wiggler and guide field case discussed here. We will follow the formalism of these references, which may be consulted for further details. We will find that the linearization of our model, under the (good) approximation that the dominant term in the field equation is the phase bunching that arises from energy changes, results in a cubic dispersion relation found previously[21] using kinetic theory.

For simplicity, the FEL equations may be written in the complex form as

$$\frac{d\gamma}{dz}=\frac{iC\beta_\perp}{2\beta_\parallel}ae^{i\theta}-\frac{i\omega_{p0}^2p_\perp^2}{c^2(k_z+k_w)}\sum_n\frac{e^{in\theta}\langle e^{-in\theta}\rangle}{n}+\text{c.c.}, \tag{24}$$

$$\frac{d\theta}{dz}=k_w+k_z-\omega/c\beta_\parallel, \tag{25}$$

$$\frac{da}{dz}=(i2\pi CI/I_A)\langle(\beta_\perp/\beta_\parallel)e^{-i\theta}\rangle, \tag{26}$$

where the complex field $a=a_se^{i\phi}$. The linearization proceeds by defining

$$\Delta K=k_w+k_z-\omega/c\beta_{\parallel 0}, \tag{27}$$

$$\theta=\theta_0+\Delta Kz+\delta\theta, \tag{28}$$

$$\gamma=\gamma_0+\delta\gamma, \tag{29}$$

$$\beta_\parallel=\beta_{\parallel 0}+\frac{\partial\beta_{\parallel 0}}{\partial\gamma}\delta\gamma, \tag{30}$$

$$\eta=2\pi CI/I_A. \tag{31}$$

The injected beam is initially unbunched:

$$\langle e^{i(\theta_0+\Delta Kz)}\rangle=0. \tag{32}$$

The dispersion relation is easily found by assuming exponential forms for the perturbations,

$$\delta\gamma=\overline{\delta\gamma}e^{i(\theta_0+\Delta Kz+\Gamma z)}+\text{c.c.}, \tag{33}$$

$$\delta\theta=\overline{\delta\theta}e^{i(\theta_0+\Delta Kz+\Gamma z)}+\text{c.c.}, \tag{34}$$

$$a=\bar{a}e^{i\Gamma z}. \tag{35}$$

Combining the equations for $\delta\gamma$ and $\delta\theta$, and averaging over the particle distribution, yields an expression for the phase bunching

$$\langle -i\overline{\delta\theta}\rangle=-\frac{\bar{a}}{\chi_\parallel}\left\langle\frac{\omega C\beta_{\perp 0}}{2c\beta_{\parallel 0}^3}\frac{\partial\beta_{\parallel 0}}{\partial\gamma}[(\Delta K+\Gamma)^2]^{-1}\right\rangle, \tag{36}$$

where

$$\chi_\parallel=1-\frac{\omega_{p0}^2p_\perp^2}{(k_z+k_w)c^2}\left\langle\frac{\omega}{c\beta_{\parallel 0}^2}\frac{\partial\beta_{\parallel 0}}{\partial\gamma}[(\Delta K+\Gamma)^2]^{-1}\right\rangle. \tag{37}$$

Note that, in the absence of the radiation field, Eq. (36) yields $\chi_\parallel=0$, which becomes, with $\omega/(k_z+k_w)\approx c\beta_{\parallel 0}$,

$$\frac{p_\perp^2\omega_{p0}^2}{\beta_{\parallel 0}(\Delta K+\Gamma)^2c^2}\frac{\partial\beta_{\parallel 0}}{\partial\gamma}=1. \tag{38}$$

Solving Eq. (38) for Γ yields the longitudinal beam plasma frequency (along with the arbitrary shift ΔK).

Employing Eq. (36) in the linearized equations for $\overline{\delta\gamma}$, $\overline{\delta\theta}$, and $\bar{a}$ results in the dispersion relation

$$-\frac{2\pi CI}{I_A\Gamma}\left(\left\langle\frac{\beta_{\perp 0}}{\beta_{\parallel 0}}\frac{\omega C\beta_{\perp 0}}{2c\beta_{\parallel 0}^3}\frac{\partial\beta_{\parallel 0}}{\partial\gamma}(\Delta K+\Gamma)^{-2}\right\rangle+\frac{\omega_{p0}^2p_\perp^2}{(k_z+k_w)c^2\chi_\parallel}\left\langle\frac{\omega C\beta_{\perp 0}}{2c\beta_{\parallel 0}^3}\frac{\partial\beta_{\parallel 0}}{\partial\gamma}(\Delta K+\Gamma)^{-2}\right\rangle\times\left\langle\frac{\beta_{\perp 0}}{\beta_{\parallel 0}}\frac{\omega}{c\beta_{\parallel 0}^2}\frac{\partial\beta_{\parallel 0}}{\partial\gamma}(\Delta K+\Gamma)^{-2}\right\rangle\right)=1. \tag{39}$$

In deriving Eq. (39), we only included the $\delta\theta$ term in the linearized a equation. There is also a $\delta\gamma$ term in the a equation which, if included, would slightly modify Eq. (39). For a cold, tenuous beam, the factor ΔK is equal for each electron, and only lowest order in ω_{p0}^2 need be retained after multiplication of Eq. (39) by $\chi_\parallel$. Then a simplified cubic dispersion relation can be derived

$$\Gamma^3+2\Delta K\Gamma^2+\left(\Delta K^2-\frac{\omega}{c\beta_{\parallel 0}^2}\frac{\partial\beta_{\parallel 0}}{\partial\gamma}\frac{\omega_{p0}^2p_\perp^2}{(k_z+k_w)c^2}\right)\Gamma+\frac{\pi C^2\beta_{\perp 0}^2I\omega}{\beta_{\parallel 0}^4cI_A}\frac{\partial\beta_{\parallel 0}}{\partial\gamma}=0. \tag{40}$$

The factor $\partial\beta_{\parallel 0}/\partial\gamma$ can be expressed, using Eqs. (4) and (5) and restricting to the limit $\lambda\ll 1$, as

$$\frac{\partial\beta_{\parallel 0}}{\partial\gamma}=\frac{1}{\gamma\beta_{\parallel 0}}\left(\frac{1}{\gamma_\parallel^2}+\frac{x}{1-x}\right), \tag{41}$$

where $\gamma_\parallel^2=1/(1-\beta_{\parallel 0}^2)$ and

$$x=c^2k_w^2a_w^2\Omega_0/(c\beta_\parallel k_w\gamma-\Omega_0)^3. \tag{42}$$

With this expression for $\partial\beta_{\parallel 0}/\partial\gamma$ the cubic dispersion relation Eq. (40) is identical to the cubic dispersion relation previously obtained by previous authors[21] and the space-charge wave may be unstable in a suitable parameter regime.[22]

IV. SPACE-CHARGE FORCES IN THE COLLECTIVE FEL

Examination of the coupled FEL equations shows that the particle bunching in the ponderomotive beat wave between the wiggler and radiation fields will result in space-charge forces which, for the low energy beam of this experiment, can be comparable in strength to the ponderomotive force.

This is apparent in Fig. 1, where the particle phase space (γ,ψ) and force $(d\gamma/dz,\psi)$ are plotted at four axial positions in the 2m wiggler. Initially, in Figs. 1(a) and 1(b), the particles are unbunched and the force is nearly zero; then, for

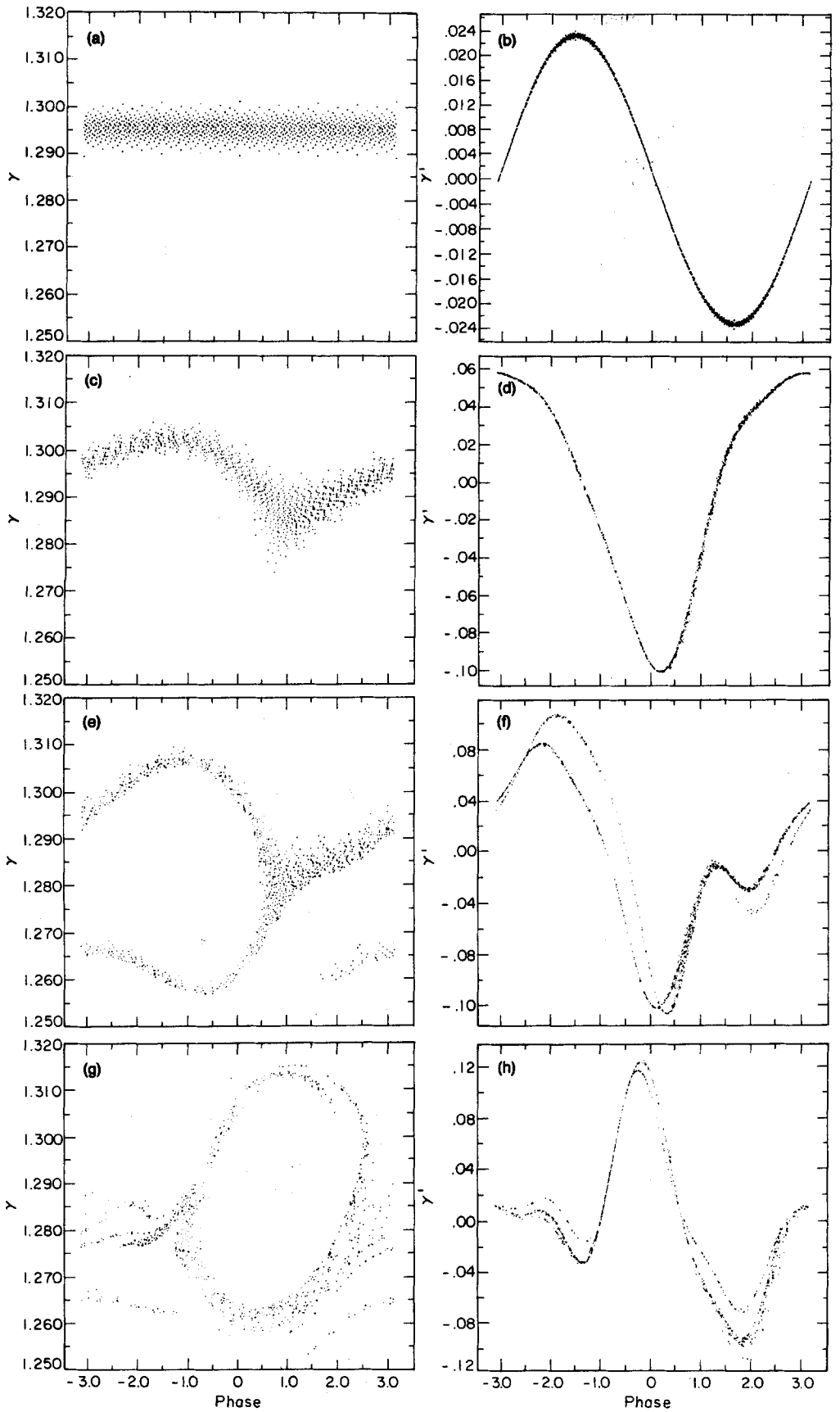

FIG. 1. Particle phase space (γ,ψ) [(a), (c), (e), (g)] and force $(d\gamma/dz, \psi)$ [(b), (d), (f), (h)] at $z = 0$ [(a), (b)], $z = 60$ cm [(c), (d)], $z = 120$ cm [(e), (f)], and $z = 180$ cm [(g), (h)].

small bunching, Figs. 1(c) and 1(d), the force is nearly sinusoidal. The power saturates near $z = 1$m, and subsequently the force has large harmonic content [Figs. 1(e) and 1(f)]. The phase space portraits are seen to be substantially distorted from the usual FEL pendulum motion, where after saturation, tight bunches would form inside clearly defined separatrix. The power and phase evolution for these runs are shown in Figs. 2(a) and 2(b).

By substituting the linear results of

$$a = a_0 \cosh(\zeta z), \tag{43}$$

and

$$\delta\theta = (a_0 I_A \beta_{\parallel 0}/\pi IC\beta_{\perp 0})\zeta \cos(\theta_0 + \Delta Kz)\sinh(\zeta z), \tag{44}$$

where ζ is the radiation field growth rate, into the linearized form of Eq. (24), one can see that the ratio of the space-charge force to the ponderomotive force,

$$\left|\frac{F_{sc}}{F_{pond}}\right| = \frac{\omega_{p0}^2 p_\perp^2 I_A \beta_{\parallel 0}^2}{c^2(k_z + k_w)\pi IC^2\beta_{\perp 0}^2}\zeta \tanh(\zeta z) \tag{45}$$

in the linear regime. Since $\omega_{p0}^2 \sim I$, the current dependence of the force ratio appears only through ζ, which goes as $I^{1/4}$. The ratio grows as a hypobolic tangent function of z with its asymptotic value evaluated by replacing $\tanh(\zeta z)$ with 1.

As an illustrating case, $P_{in} = 1$ W, $I = 1$ A, $B_w = 188$ G, $B_\parallel = 1500$ G, and other experimental parameters the same as that described later in Sec. V, the input power is small enough to ensure that the FEL interaction remains linear throughout the entire length of the laser. Here ζ is found to be 1.35 in linear theory. The ratio of the space-charge force to the ponderomotive force, $|F_{sc}/F_{pond}|$, evaluated using Eq. (45), increases from 0 at the entrance to 87% of its asymptotic value of 1.7 at $z = 1$ m, and to 99 % at $z = 2$ m. A gain, $G \equiv P_{out}/P_{in}$, of 56 at $z = 2$ m is found in simulation. With the space-charge force artificially turned off, the gain increases to 750 at $z = 2$ m. So it is clear that there is a large reduction in the small signal gain due to the space-charge effect in the linear regime.

The strong influence of the space-charge forces on the particle motion is illustrated in Figs. 3(a) and 3(b). Here the electrons are injected at the resonant energy, where the Raman regime FEL gain is small. The input power is sufficient to produce at least one synchrotron oscillation during the interaction. At high current, the space charge is strong enough to debunch the beam, and the particles oscillate only slightly [Fig. 3(a)], while at low current, the particles move on pendulumlike orbits (Fig. 3(b)]. Approximating the space-charge wave with only one harmonic yields results different from the simulation (which includes four harmonics) by a few percent before saturation, and by 10%–15% after saturation. Efficiency enhancement schemes are also rendered more difficult by the space-charge debunching. For the low wiggler fields of this experiment, the product

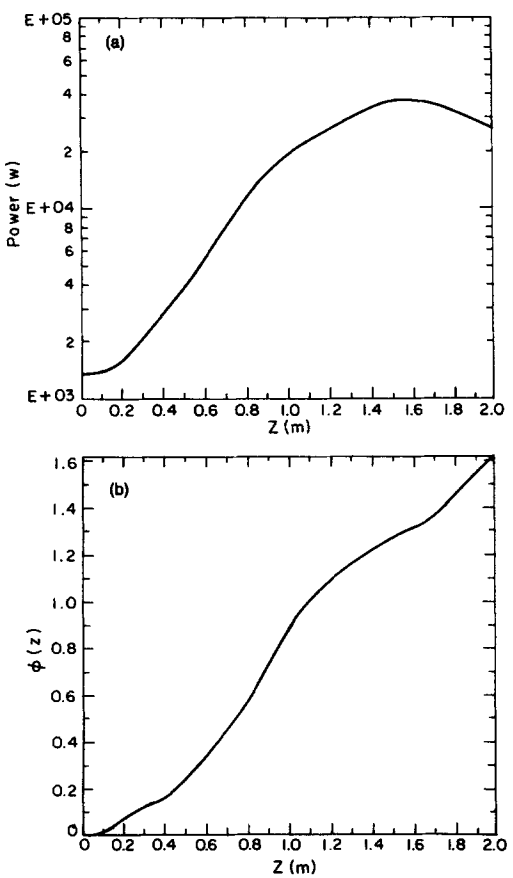

FIG. 2. The rf power (a) and rf phase (b) versus interaction length z for the simulation shown in Fig. 1.

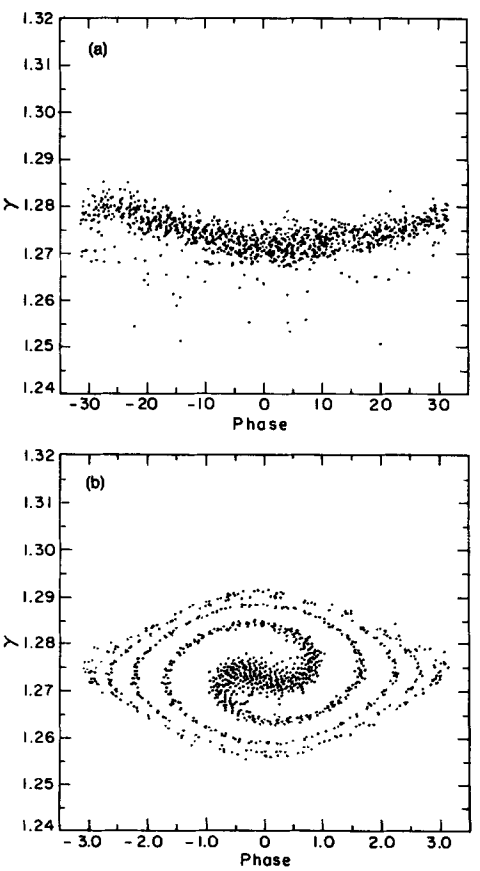

FIG. 3. Particle phase space (γ,ψ) with injection at the ponderomotive velocity (zero detuning). Here $B_w = 188$ G, $B_\parallel = 1510$ G, $P_{in} = 4$ kW, and $z = 6$ m. In (a), $I = 3.3$ A. In (b), $I = 0.01$ A.

$\gamma\beta_\perp \ll 1$, and efficiency enhancement must rely on a wiggler wavelength downtaper. Numerous numerical schemes were examined and, for our typical system parameters, detrapping during the taper severely limited the efficiency. Thus our studies indicate that a FEL operating deep in the Raman regime will be difficult to taper.

V. COMPARISONS WITH EXPERIMENT

The FEL experiment has been described in detail elsewhere,[5,6] and the reader may consult these references for a detailed description of the apparatus. Free electron laser physics is studied here by measuring the output rf power with varying beam energy, beam current, wiggler field, input rf power level, and interaction length. The wiggler has a 3.3 cm period with an adiabatic entrance over six periods. The length of the interaction region is adjusted by an axially moveable "kicker" magnet that deflects the beam into the waveguide wall.

The input power source is a 9.3 GHz high power (~ 30 kW) short pulse magnetron, which saturates the FEL at approximately 1 m. The axial location of saturation can be shifted by changing the wiggler field, as shown in Fig. 4, where the power is plotted as a function of axial position for three wiggler field amplitudes. The general behavior of the experiment is reproduced by the theory, but at the stronger wiggler fields the experimental measurements are larger than predicted by $\sim 15\%$.

The putput powers shown in Fig. 4 are for the fixed beam voltage V that gives the greatest gain at the entrance of the wiggler ($z \lesssim 60$ cm). We find that the voltage that yields the maximum output power increases steadily for interaction lengths longer than the saturation length. At the peak gain voltage, the FEL saturates at approximately $z \approx 115$ cm, after which a synchrotron oscillation causes the output power to decrease. As shown by the simulations of Fig. 5, at higher beam voltages the FEL interaction proceeds more slowly, and saturation is delayed past $z = 115$ cm. Thus at large z the output power is maximized at higher beam voltages.

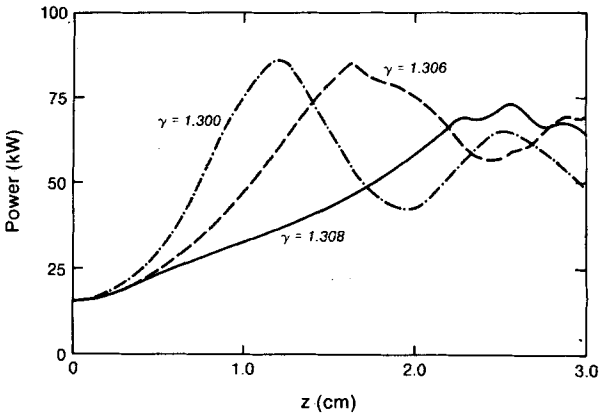

FIG. 5. Simulation of rf output power versus interaction length z for three values of beam energy.

This phenomenon is shown experimentally in Figs. 6 and 7. In Fig. 6, we plot the output power as a function of beam voltage for three axial positions. In both the data and the simulation, the voltage corresponding to peak gain increases $\sim 2\%$ as z increases from 81 cm to 155 cm. Figure 7 shows the voltage for peak gain as a function of interaction length between $z = 81$ and 155 cm.

The peak gain voltage depends on axial position past saturation. In addition, at high power, nonlinear phenomena

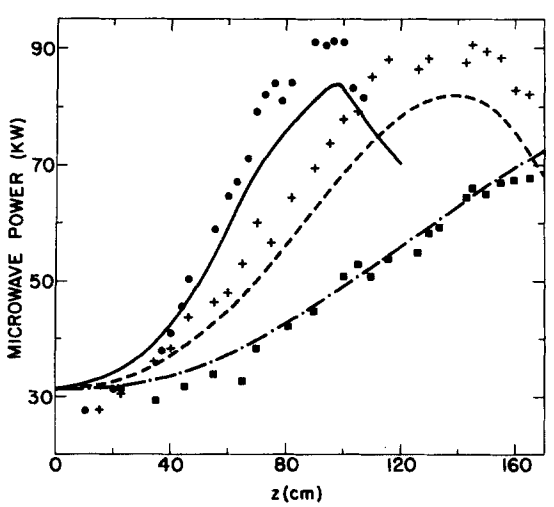

FIG. 4. Power as a function of interaction length z for three values of wiggler fields. Circles ($B_w = 243$ G), crosses ($B_w = 173$ G), and squares ($B_w = 115$ G) are from the experiment. The lines are from simulation. Here $B_\parallel = 1450$ G, $I = 3.5$ A, $P_{in} = 32$ kW, and $f = 9.3$ GHz.

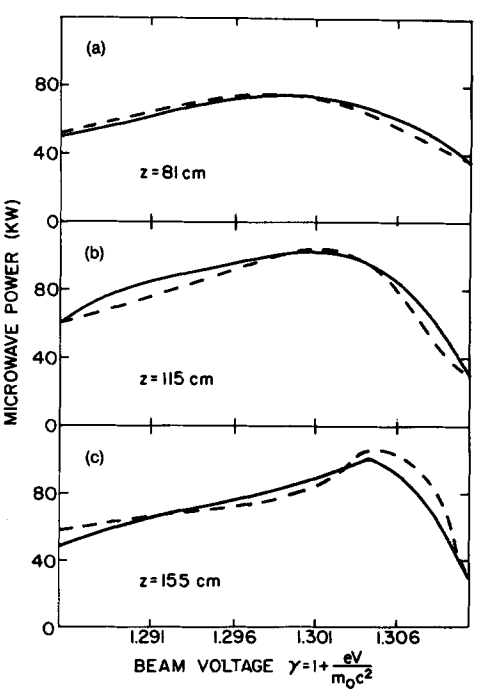

FIG. 6. Power versus beam energy γ for three values of the interaction length z. The solid lines are from the experiment. The dashed lines are from simulation. Here $B_w = 187$ G, $B_\parallel = 1470$ G, $I = 4.5$ A, $P_{in} = 32$ kW, and $f = 9.3$ GHz.

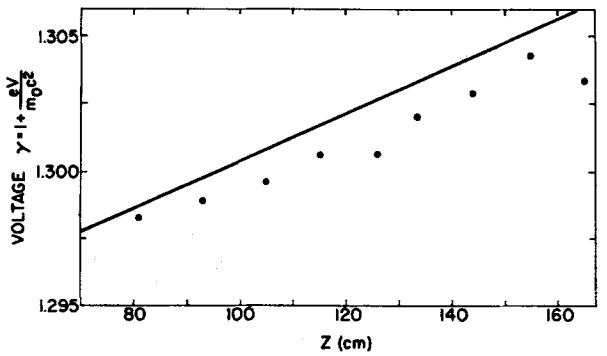

FIG. 7. Voltage (γ) for peak gain versus interaction length z. The dots are from the experiment and the line is from simulations. Here $B_w = 187$ G, $B_\parallel = 1470$ G, $I = 4.5$ A, $P_{in} = 16$ kW, and $f = 9.3$ GHz.

exist well before saturation ($z \lesssim 60$ cm). These effects cause the voltage that gives the maximum output power to differ from both the predictions of linear theory and from measurements at small input signals. For example, at 30 kW the computed beam energy that maximizes the unsaturated gain is approximately 2% higher than is found with small signal linear theory. This effect is explained schematically in Fig. 8. The electron beam energy corresponding to peak linear gain γ_g is, in the Raman regime, upshifted from the resonant energy γ_r by a factor proportional to the beam plasma frequency. When the input power is small, the ponderomotive potential bucket height, given by

$$h_{\text{bucket}} = 2\sqrt{\frac{C\beta_{\parallel r}\beta_{\perp r}a_s c}{\omega(\partial\beta_{\parallel r}/\partial\gamma_r)}}\,, \tag{46}$$

where $\beta_{\parallel r}$ and $\beta_{\perp r}$ are the values of $\beta_\parallel$ and $\beta_\perp$ at the resonant energy, is also small compared to $\gamma_g - \gamma_r$. In this case the input beam energy corresponding to maximum unsaturated output power is the γ_g from linear theory. However, when the input power is increased sufficiently, the trapping bucket approaches the linear optimized beam energy γ_g. When this occurs the output power can be increased by increasing the beam energy above the energy γ_g predicted by linear theory.

This effect is observed experimentally and is reproduced in the simulations. The dashed line in Fig. 9 is the computed

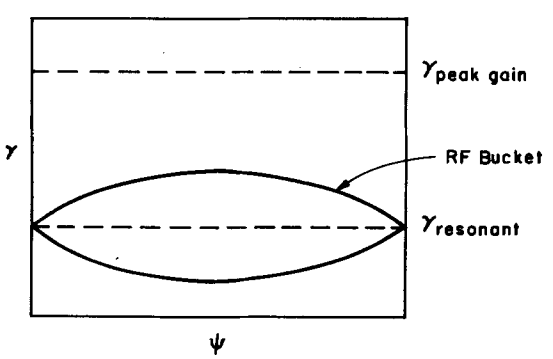

FIG. 8. Schematic of the ponderomotive bucket.

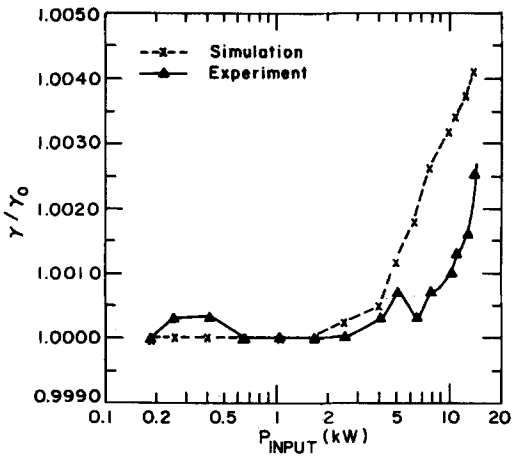

FIG. 9. Normalized voltage (γ) for peak gain versus input power P_{in}. Here $z = 115$ cm, $B_w = 188$ G, $B_\parallel = 1500$ G, $I = 3.3$ A, and $f = 9.3$ GHz.

energy for peak gain as a function of the input power. For low power, the peak gain energy is equal to the linear regime peak gain energy. However, when the power is sufficiently large (the bucket height is of order $\gamma_g - \gamma_r$), the input energy corresponding to peak gain increases.

Efficiency measurements constitute another test of nonlinear FEL theory. We find that the well-known[13] theoretical collective regime efficiency scaling with current, $\eta \propto I^{1/2}$ is not observed for high input power and low beam current. Linear theory predicts that the difference $\gamma_g - \gamma_r$ also scales as $I^{1/2}$. As indicated in Fig. 8, when the beam current is reduced, the γ_g of linear theory moves inside the ponderomotive bucket at $z = 0$, and then the peak gain energy is no longer γ_g. Under these conditions, experiments and simulations show that more power can be extracted by increasing the initial beam energy. The efficiency is then only a weak function of the current. In Fig. 10 we plot the numerically predicted efficiency. on log–log scales, for two input powers, as a function of the beam current. The low input power line, marked with the dots, is linear. The high input power plot,

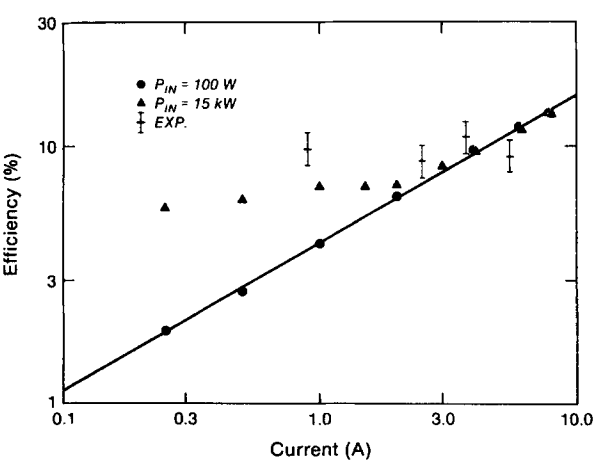

FIG. 10. Peak efficiency η versus beam current I. The triangles and circles are from the simulation, and the line is the graph of the simplistically predicted $\eta \propto I^{1/2}$ dependence. Here $B_w = 188$ G, $B_\parallel = 1510$ G, and $f = 9.3$ GHz.

marked by triangles, is linear at high current, but flattens at low current. The experimentally observed efficiency,[6] marked by the crosses, is taken at high power only. As expected, the efficiency is roughly flat over the measured beam current range.

VI. CONCLUSIONS

We find that this measurements of the spatial rf growth, saturation, and subsequent decay in this collective (Raman) FEL amplifier are explained by a nonlinear theory that takes into account electron trapping in the potential wells formed by the combined action of the ponderomotive and beam space-charge forces. Scaling of the power and efficiency with electron beam current and voltage are likewise in agreement with theoretical predictions.

Many of the results presented in this paper are for input powers comparable to the output power; however, despite appearances, this is not an artificial regime. It is, in fact, precisely the operating regime of a low gain, multipass oscillator. The various energy shifts and scaling law changes demonstrated in this paper must be carefully considered when optimizing the behavior of such an oscillator.

ACKNOWLEDGMENTS

Some of this work was performed at the University of California, San Diego.

This work was supported by the National Science Foundation, the Office of Naval Research, the Air Force Office of Scientific Research, and the Hertz Foundation.

[1]H. Motz, J. Appl. Phys. **22**, 527 (1951).
[2]R. M. Phillips, IRE Trans. Electron. Devices **ED-7**, 231 (1960).
[3]L. R. Elias, W. Fairbank, J. Madey, H. A. Schwettman, and T. Smith, Phys. Rev. Lett. **36**, 717 (1976).
[4]T. J. Orzechowski, E. T. Scharlemann, B. Anderson, V. K. Neil, W. M. Fawley, D. Prosnitz, S. Yarema, D. B. Hopkins, A. C. Paul, A. M. Sessler, and J. S. Wurtele, IEEE J. Quantum Electron. **QE-21**, 831 (1985).
[5]J. Fajans, G. Bekefi, Y. Z. Yin, and B. Lax, Phys. Rev. Lett. **53**, 246 (1984); J. Fajans and G. Bekefi. Phys. Fluids **26**, 1995 (1985).
[6]J. Fajans, J. S. Wurtele, G. Bekefi, D. K. Knowles, and K. Xu, Phys. Rev. Lett. **57**, 579 (1986).
[7]T. J. Orzechowski, B. R. Anderson, J. C. Clark, W. M. Fawley, A. C. Paul, D. Prosnitz, E. T. Scharlemann, S. M. Yarema, D. B. Hopkins, A. M. Sessler, and J. W. Wurtele, Phys. Rev. Lett. **57**, 2172 (1986).
[8]W. B. Colson, IEEE J. Quantum Electron. **QE-17**, 1417 (1981).
[9]N. M. Kroll, P. L. Morton, and M. R. Rosenbluth, IEEE J. Quantum Electron. **QE-17**, 1436 (1981).
[10]D. Prosnitz, A. Szoke, and V. K. Neil, Phys. Rev. A **24**, 1436 (1981).
[11]J. S. Wurtele, E. T. Scharlemann, and A. M. Sessler, Nucl. Instrum. Methods A **250**, 176 (1986).
[12]J. Byers and R. Cohen, Nucl. Instrum. Methods A **272**, 595 (1988).
[13]H. P. Freund, S. Johnston, and P. Sprangle, IEEE J. Quantum Electron. **QE-19**, 322 (1983).
[14]J. Fajans, D. Kirkpatrick, and G. Bekefi, Phys. Rev. A **32**, 3448 (1985).
[15]G. M. Branch and T. G. Mihran, IRE Trans. Elec. Dev. **ED-2**, 3 (1955).
[16]J. Fajans and J. S. Wurtele, Phys. Fluids B **1**, 2073 (1989).
[17]E. Jerby and A. Gover, Nucl. Instrum. Methods A **272**, 380 (1988).
[18]S. Y. Cai, A. Bhattacharjee, and T. C. Marshall, IEEE J. Quantum Electron. **QE-23**, 1651 (1987).
[19]R. Bonifacio, C. Pelligrini, and L. M. Narducci, Opt. Commun. **50**, 373 (1984).
[20]H. Saito and J. S. Wurtele, Phys. Fluids **30**, 2209 (1987).
[21]L. Friedland and A. Fruchtman, Phys. Rev. A **25**, 2693 (1982).
[22]H. Freund and P. Sprangle, Phys. Rev. A **28**, 1835 (1983).